Development of Fe2O3-based, Al2O3-stabilized Oxygen Carriers using Sol-gel Technique for H2 Production via Chemical Looping

Author(s):
Yüzbasi, Nur S.; Kierzkowska, Agnieszka; Müller, Christoph

Publication date:
2017-07

Permanent link:
https://doi.org/10.3929/ethz-b-000179351

Originally published in:
Energy Procedia 114, https://doi.org/10.1016/j.egypro.2017.03.1186

Available online at www.sciencedirect.com

ScienceDirect

Energy Procedia 114 (2017) 436 – 445

Energy Procedia

13th International Conference on Greenhouse Gas Control Technologies, GHGT-13, 14-18 November 2016, Lausanne, Switzerland

Development of Fe_2O_3-based, Al_2O_3-stabilized oxygen carriers using sol-gel technique for H_2 production via chemical looping

Nur Sena Yüzbasi[a], Agnieszka Kierzkowska[a], Christoph Müller[a,] *

[a] Laboratory of Energy Science and Engineering, Institute of Energy Technology, ETH Zurich, Zurich, 8092, Switzerland

Abstract

A modification of the chemical looping combustion (CLC) process allows the production of high purity hydrogen from biomass (with simultaneous CO_2 capture) on the distributed scale. Here, we report the development of Fe_2O_3-based, Al_2O_3-supported oxygen carriers using a sol-gel technique. We assess the influence of the iron precursor on the morphological properties, chemical composition and cyclic redox stability of the oxygen carrier. Three iron precursors, i.e. iron nitrate, iron chloride and iron acetylacetonate, were used to synthesize oxygen carriers containing 80 wt. % of Fe_2O_3. Using iron nitrate and iron acetylacetonate as the iron precursor resulted in materials with a high H_2 yield. However, both materials showed some decay in the hydrogen yield with cycle number. Al_2O_3-stabilized Fe_2O_3 synthesized using iron chloride as the iron precursor showed no appreciable decay over the 15 cycles tested, albeit the amount of hydrogen produced was significantly lower when compared to the other two iron precursors. This observation can be attributed to the large fraction of hercynite ($FeAl_2O_4$) in this material. Hercynite stabilizes iron and prevents sintering, but does not participate in the redox reactions.

Peer-review under responsibility of the organizing committee of GHGT-13.

Keywords: Chemical looping combustion; sol-gel; Fe_2O_3; hydrogen production.

* Corresponding author. Tel.: +41 44 632 3440.
E-mail address: muelchri@ethz.ch

Peer-review under responsibility of the organizing committee of GHGT-13.
doi:10.1016/j.egypro.2017.03.1186

1. Introduction

A modification of the conventional chemical looping process allows for the production of high purity hydrogen from a carbonaceous fuel while capturing simultaneously CO_2 [1-3]. Here, in the first step a carbonaceous fuel is gasified yielding a mixture of predominantly CO, H_2, CO_2, H_2O and CH_4. In the second step, the synthesis gas reduces iron oxide to a lower oxidation state, producing thereby a mixture of CO_2 and H_2O. After condensation of steam a pure stream of CO_2 is obtained. In the third step, H_2 of high purity is obtained by re-oxidation of metallic iron with steam. The cycle is closed through the oxidation of Fe_3O_4 to Fe_2O_3 with air [3-7].

It has been demonstrated that pure iron oxide deactivates after only a few redox cycles when Fe_2O_3 is fully reduced to Fe [1, 5]. The stabilization of iron oxide on a support, e.g. aluminum oxide, zirconium oxide, titanium oxide or magnesium oxide has been proposed to reduce the extent of this deactivation mechanism [2-9].

So far several synthesis techniques including mechanical mixing, freeze granulation, impregnation and co-precipitation have been used to synthesize Fe_2O_3-based, Al_2O_3-supported oxygen carriers [4, 10, 11]. However, two common limitations of these methods are the low surface area of the material prepared and that mixing between the active component (Fe_2O_3) and the support occurs on a macroscopic level only (resulting often in poor homogeneity of the materials synthesized). On the other hand, in the area of catalysis the sol-gel method has received significant attention since it allows for the homogeneous mixture of components on the molecular level [12]. In addition, by manipulation of the sol-gel parameters, e.g. pH or precursors, the porous structure of the material can be adjusted. Recently, sol-gel approaches have been introduced into chemical looping combustion research. For example, Li et al. [13] synthesized Fe_2O_3-based oxygen carriers that showed a high reactivity and redox-stability over more than 100 cycles. The average purity of the hydrogen produced was 99.8%. Similarly, using a sol-gel technique Kierzkowska et al. [3] prepared several Al_2O_3 supported oxygen carriers with a varying ratio of Fe_2O_3 to Al_2O_3 (0.6-0.9). It was reported that the oxygen carrier that contained 60 wt. % Fe_2O_3 possessed a stable H_2 yield of 7.5 mmol/gram over 40 cycles. The stability of the oxygen carrier was attributed to the formation of the spinel $FeAl_2O_4$ (hercynite). The thermodynamically limited re-oxidation of $FeAl_2O_4$ with steam explained the lower than expected hydrogen yield. However, oxidation in air re-oxidized $FeAl_2O_4$ back to Fe_2O_3 and Al_2O_3.

It is well known that the sol-gel parameters, e.g. the pH value or precursors affect critically the rates of the hydrolysis and condensation reactions and, in turn, the morphology of the synthesized materials. Thus, the aim of this study was to assess critically the influence of the iron precursor on the morphology and in turn the redox characteristics of oxygen carriers for CL-based hydrogen production.

2. Experimental

2.1 Synthesis of the oxygen carriers

Oxygen carriers with a mass ratio of Fe_2O_3 to Al_2O_3 of 80:20 were synthesized via a sol-gel method based on the synthesis protocol reported by Kierzkowska et al [3]. In a typical synthesis, aluminum isopropoxide was mixed with water and the mixture was hydrolyzed for two hours at 75 °C under constant stirring. Nitric acid was used to peptize the slurry. The required amount of the iron precursor was mixed with water to obtain a 1 M solution that was added subsequently to the slurry and refluxed for 12 h at 90 °C. The following iron precursors were used: iron nitrate ($Fe(NO_3)_3 \cdot 9H_2O$), iron chloride ($FeCl_3 \cdot 6H_2O$) and iron acetylacetonate ($Fe(C_5H_7O_2)_3$). The molar ratio of Al^{+3}:H_2O:H^+ was fixed to 0.5:50:0.07. The resulting gel was dried at 100 °C overnight to remove the encapsulated solvents. A xerogel was obtained after calcination at 900 °C for 2 hours. The calcined material was crushed and sieved to a particle size range 300 – 425 µm for further characterization. The following nomenclature is used to describe the oxygen carriers: FeAl-nitrate, FeAl-chloride and FeAl-acac for the oxygen carriers synthesized using $Fe(NO_3)_3 \cdot 9H_2O$, $FeCl_3 \cdot 6H_2O$ and $Fe(C_5H_7O_2)$, respectively.

2.2 Characterization of the oxygen carriers

The chemical composition of the calcined oxygen carriers was characterized by X-ray diffraction (XRD) using a Bruker AXS D8 Advance X-ray diffractometer mounted with a Lynxeye superspeed detector, operated at 40 kV and 40 mA (CuKα radiation). The step size was 0.275 °/s and diffraction patterns were recorded in the range of 2θ = 20-80 °.

Oxygen carriers were characterized further by scanning electron microscopy (Zeiss Gemini 1530 FEG) before and after reactive tests. Prior to imaging, the samples were sputter coated (MED 010) with an approximately 10 nm thick layer of platinum

The surface area and pore size distribution of the calcined oxygen carriers were determined using a Quantochrome NOVA 4000e N_2 adsorption analyzer. Prior to the acquisition of the N_2 isotherms, the samples were degassed at 300 °C for two hours. BET and BJH models were used to calculate, respectively, the surface area and the pore size distribution of the materials [14, 15].

H_2 temperature programmed reduction (TPR) were performed in a thermogravimetric analyzer (TGA, Mettler Toledo TGA/DSC 1). In a typical experiment ~ 30 mg of the oxygen carrier was placed in an alumina crucible. The flow rate of hydrogen (10 vol. % H_2 in N_2) and the purge stream over the micro-balance (N_2) were 100 ml/min and 25 ml/min, respectively. The sample was heated from 25 to 1050 °C using a temperature ramp of 10 °C/min. Subsequently, the sample was held at 1050 °C for 30 minutes.

The cyclic redox performance of the oxygen carriers was assessed in a fixed bed (Fig 1). The fixed bed was constructed of recrystallized Al_2O_3 and had an internal diameter of 20 mm (length 590 mm). A frit containing 5 holes (hole diameter 1.5 mm) was located 200 mm from the bottom of the reactor. First, the bed was loaded with 3.5 g of coarse Al_2O_3 (1400-1700 µm), followed by an approximately 10 mm long plug of quartz wool. Subsequently, 0.5 g of the oxygen carrier, mixed with 5 g of Al_2O_3 (300-425 µm) were placed on top of the plug of quartz wool. Finally 10 grams of coarse alumina (1400-1700 µm) were added. The layer of coarse alumina and the quartz wool plug in the bottom of the bed prevented oxygen carriers from falling through the holes of the frit. The top layer of coarse alumina preheated effectively the gas entering the bed.

The reactor was placed in a tubular furnace. The temperature of the bed was controlled via a N-type thermocouple placed inside the layer containing the oxygen carrier. The flow rate of carbon monoxide was metered with a calibrated rotameter, whereas the flowrates of carbon dioxide, air and nitrogen were recorded via calibrated mass flow meters (AWM5101VN, Honeywell). The switching between the different gas atmospheres was performed using a computer-controlled setup comprising 6 solenoid valves. Water was fed via a syringe pump (0.3 ml/min) to an electrically heated vaporizer maintained at 210 °C. A typical redox cycle comprised the following steps: (i) reduction in CO (10 % CO and 10 % CO_2 in N_2) for 15 minutes (1.5 L/min), (ii) purging with N_2 (1.5 L/min) for 1 minute, (iii) oxidation of the reduced oxygen carrier with steam (23 % H_2O in N_2) for 7 minutes (1.94 L/min), (iv) purge with N_2 (1.5 L/min) for 1 minute and (v) oxidation with 5% O_2 in N_2 (2 L/min) for 5 minutes. The gas stream leaving the packed bed was passed first through three impinger tubes, immersed in an ice bath, followed by a $CaCl_2$ drying tube, to remove unreacted steam prior to gas analysis. The composition of the gas stream leaving the packed bed was determined using the following analyzers: (i) non-dispersive infrared analyzer determining the volume fraction of CO, CH_4 and CO_2 (ABB, Uras26), (ii) non-dispersive infrared analyzer measuring CO in the range 0 – 5000 ppmv, (iii) paramagnetic analyzer determining the molar fraction of O_2 and (iv) thermal conductivity analyzer measuring H_2 (ABB, Caldos 27).

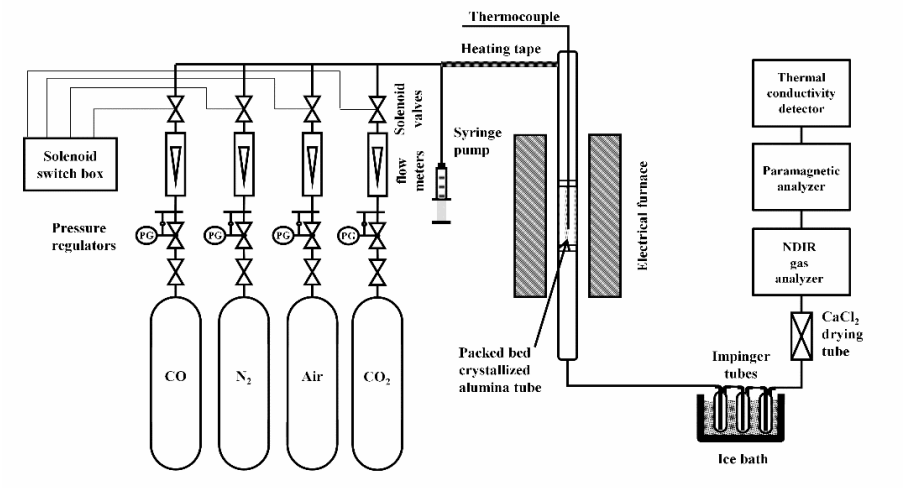

Fig. 1. Schematic diagram of the fixed bed set-up and reactor design

3. Results and discussion

3.1 Characterization of the freshly calcined materials

The composition of the freshly calcined materials was determined using X-ray diffraction (Fig. 2). Without exception, all oxygen carriers calcined at 900 °C contained corundum ($\alpha - Al_2O_3$) and hematite (Fe_2O_3). Only FeAl-chloride showed also the presence of hercynite ($FeAl_2O_4$).

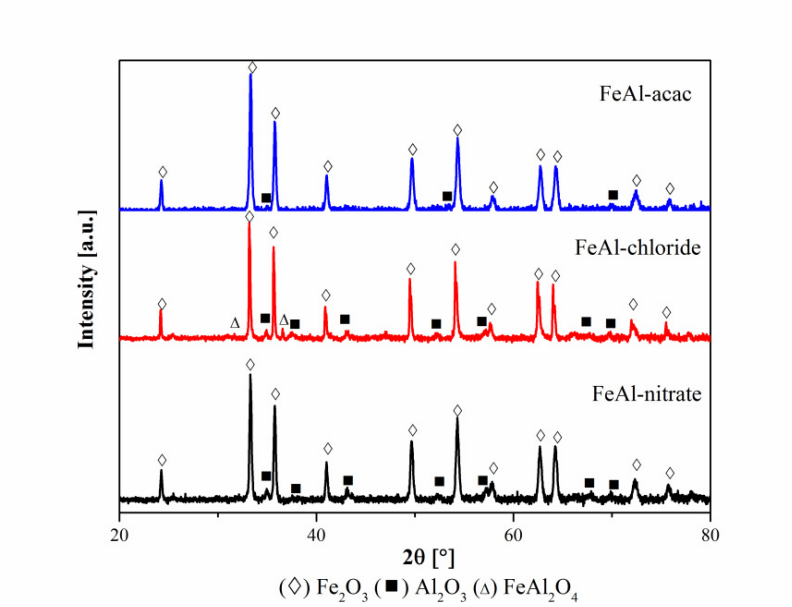

Fig. 2. XRD patterns of the materials calcined at 900 °C for 2 h.

The surface morphology of the freshly calcined materials was characterized by SEM and is shown in Fig. 3. The electron micrograph of FeAl-acac shows a homogenous and nanostructured surface (Fig. 3c). The average grain size of FeAl-acac was 78 ± 24 nm (based on the analysis of 30 grains). Also FeAl-nitrate displayed a homogenous surface morphology, composed of slightly larger grains when compared to FeAl-acac, viz the average grain size was 107 ± 34 nm. On the other hand using iron chloride as the iron precursor resulted in a heterogeneous surface structure, containing partially sintered grains.

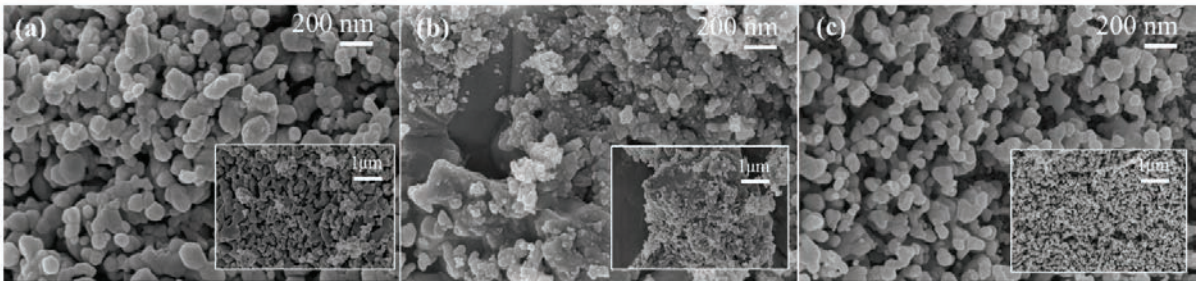

Fig. 3. Scanning electron micrographs of the calcined oxygen carriers (a) FeAl-nitrate, (b) FeAl-chloride and (c) FeAl-acac.

Table 1 summarizes the BET surface areas and Barrett-Joyner-Halenda (BJH) pore volumes of the different oxygen carriers synthesized. The measurements show that the iron precursor influenced appreciably the surface area and pore volume of the calcined materials. The oxygen carrier synthesized using iron chloride as the iron precursor possessed the largest surface area of 22 m^2 /g and pore volume 0.19 cm^3 /g. Oxygen carriers synthesized using iron nitrate as the iron precursor had the smallest BET surface area of 9 m^2 /g.

Table 1. BET surface area and BJH pore volume and pore diameter of the calcined materials.

	Surface area (m^2/g)	Pore volume (cm^3/g)
FeAl-nitrate	9	0.16
FeAl-chloride	22	0.19
FeAl-acac	16	0.16
Al_2O_3 xerogel	226	0.3

The H_2-TPR profiles of the synthesized oxygen carriers are given in Fig. 4. The reduction of the oxygen carriers started at ~ 400 °C, independent of the iron precursor. The reduction of FeAl-nitrate was slightly faster than that of FeAl-acac. However, the reduction of FeAl-chloride did not reach completion within the experimental time possibly due to the formation of $FeAl_2O_4$,

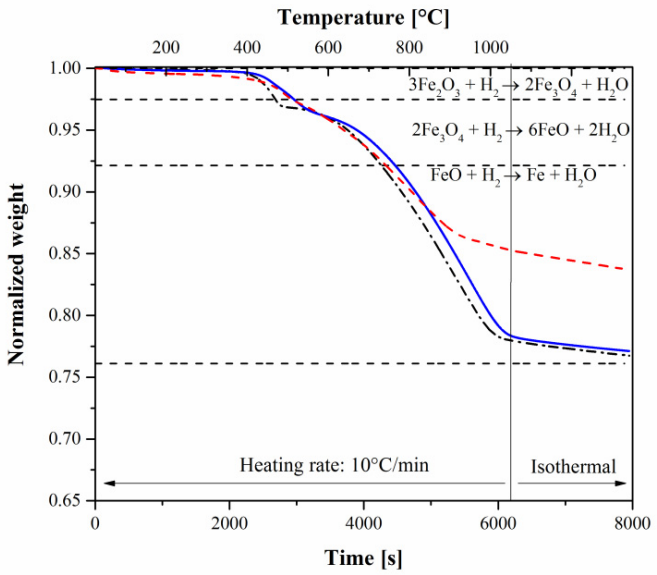

Fig. 4 H_2-temperature programmed reduction of the oxygen carriers: (-·-) FeAl-nitrate (- - -) FeAl-chloride and (▬) FeAl-acac

3.2 Redox performance of the synthesized oxygen carriers

The redox characteristics of the synthesized oxygen carriers were evaluated over 15 cycles at 800 °C in a fixed bed. Fig. 5 plots the H_2 yield, expressed as mmol hydrogen/g oxygen carrier, as a function of the cycle number. Fig. 5 confirms clearly that the cyclic hydrogen yield is influenced strongly by the iron precursor used during synthesis. The average H_2 yield per gram of oxygen carrier was determined as 12. 6 mmol H_2/g for FeAl-nitrate, 6.9 mmol H_2/g for FeAl -chloride and 11.1 mmol H_2/g for FeAl-acac. We observe that FeAl-nitrate and FeAl-acac follow similar trends in terms of redox stability. Initially, both oxygen carriers had a high H_2 yield (indeed close to the theoretically expected value). However, after approximately six redox cycles, the H_2 yield decreased. On the other hand, the oxygen carrier synthesized using iron chloride as the precursor gave stable H_2 yields over the 15 redox cycles tested, however, the quantity of hydrogen produced was substantially below the theoretically expected value of 13.4 mmol H_2/g oxygen carrier.

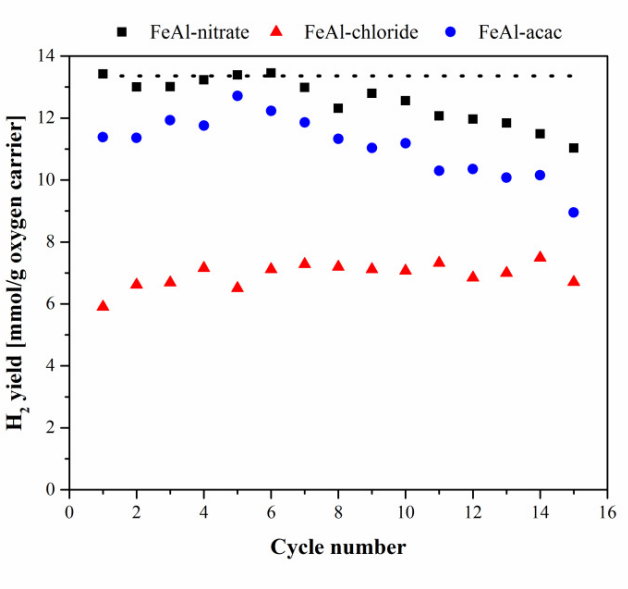

Fig. 5 H_2 yield as a function of cycle number: (■) FeAl-nitrate, (▲) FeAl-chloride and (●) FeAl-acac. The dashed horizontal line gives the theoretical quantity of H_2 expected, i.e. 13.4 mmol H_2/g for an oxygen carrier containing 80 wt. % Fe_2O_3 (assuming full reduction to Fe).

3.3 Characterization of the cycled materials

The X-ray diffractograms of the cycled oxygen carriers (reduced state) are shown in Fig. 6. A mixture of Fe_3O_4, $FeAl_2O_4$ and Fe was observed after reduction, independent of the precursor used. The presence of magnetite in the reduced oxygen carriers indicates that in the 15th cycle the oxygen carriers were only reduced partially under the conditions studied here (800 °C, 15 mins. using 10 % CO in N_2). Wüstite (FeO) was not detected in the X-ray diffractograms. Instead, FeO seems to form a solid solution with Al_2O_3, viz. hercynite ($FeAl_2O_4$). This observation is in agreement with the Fe-Al-O phase diagram reported by Kidambi et. al. [9]. The formation of hercynite is thermodynamically favored for $8 \times 10^{-2} < P_{CO2}/P_{CO} < 1.8 \times 10^5$ and $1 \times 10^{-2} < P_{H2O}/P_{H2} < 2.1 \times 10^5$ [9]. However, the formation of the iron-alumina spinel is undesirable since the oxidation of $FeAl_2O_4$ with steam is thermodynamically limited [3, 9].

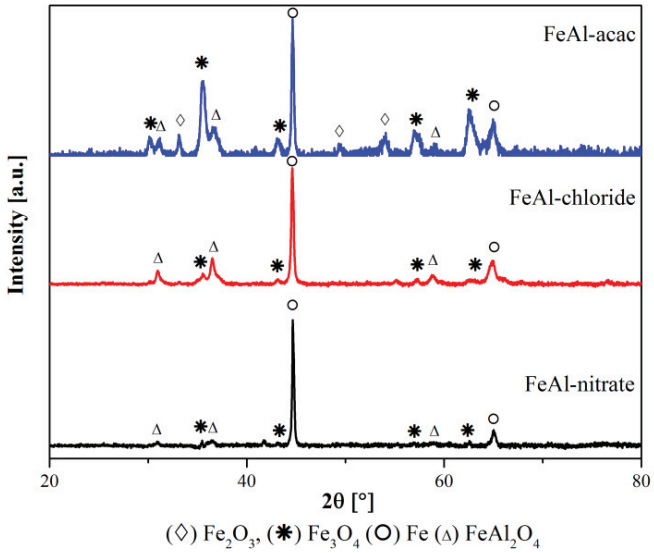

Fig. 6 XRD patterns of the oxygen carriers (reduced state) after having been subjected to 15 redox cycles.

SEM confirmed that the oxygen carriers are subject to morphological changes over multiple redox cycles (Fig. 7). For example, FeAl-nitrate and FeAl-acac reveal a severely altered surface morphology when compared to the fresh materials. The changes of the surface morphology of FeAl-chloride with cycle number are less pronounced. Over 15 redox cycles the grain size of FeAl-nitrate and FeAl-acac increased to 200 ± 59 and 191 ± 44 nm (based on the analysis of 30 grains), respectively. In comparison, the particle size of FeAl-chloride was determined as 87 ± 30 nm, approximately half the size of the grains of FeAl-nitrate and FeAl-acac.

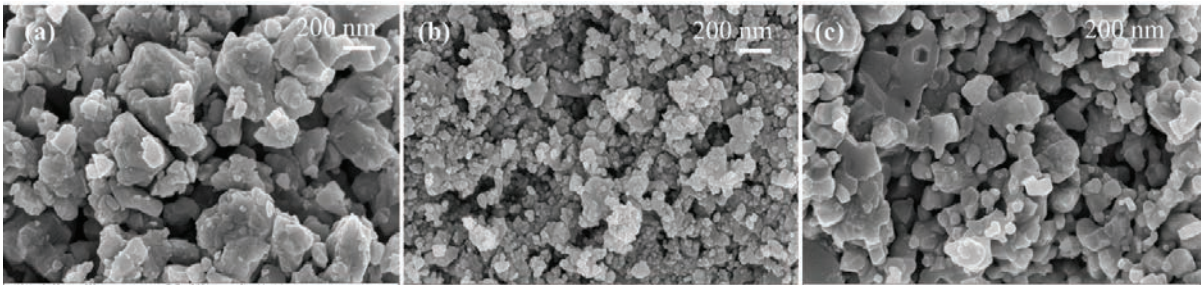

Fig. 7 Electron micrographs of oxygen carriers that have undergone15 redox cycles: (a) FeAl-nitrate, (b) FeAl-chloride and (c) FeAl-acac.

It is convincible that material sintering reduces the apparent rates of reduction, leading to incomplete reduction and reduced H_2 yields, thus, explaining the reducing H_2 yield with cycle number of FeAl-nitrate and FeAl-acac. A possible explanation for the lower sintering tendency of FeAl-chloride could be the comparatively large fraction of hercynite in this material, effectively stabilizing iron. Rietveld refinement (Table 2) confirmed that FeAl-chloride contained a larger quantity of hercynite when compared to FeAl-nitrate and FeAl-acac. The Rietveld refinement indicated a high hercynite formation in FeAl-chloride.

Table 2. Phase compositions of the oxygen carriers (cycled and reduced state) quantified by Rietveld refinement.

	Fe_2O_3 [wt. %]	Fe_3O_4 [wt. %]	$FeAl_2O_4$ [wt. %]	Fe [wt. %]
FeAl-nitrate	9.6	3.1	32	55.3
FeAl-chloride	-	6.7	55.7	37.9
FeAl-acac	15.7	40.3	24.3	19.6

4. Conclusions

In this study, Fe_2O_3-based, Al_2O_3-supported oxygen carriers were synthesized via a sol-gel technique using three different iron precursors i.e. iron nitrate, iron chloride and iron acetylacetonate. The oxygen carriers that were synthesized using either iron nitrate or iron acetylacetonate showed a high initial hydrogen yield, close to theoretically expected value of 13.4 mmol H_2/g oxygen carrier. However, the hydrogen decreased with cycle number possibly due to a sintering-induced loss in active surface area. On the other hand, the oxygen carrier that was synthesized using iron chloride as an iron precursor, showed a lower, yet stable H_2 yield over 15 cycles. The stability of this oxygen carrier was attributed to the formation of hercynite, effectively stabilizing iron oxide.

Acknowledgements

The authors are grateful to the Swiss National Science Foundation (406640_136707) and the Swiss Office of Energy (BFE) for financial support. We also thank Mrs. Lydia Zehnder for her help with the XRD analysis and the Scientific Centre for Optical and Electron Microscopy (ScopeM) for providing training on and access to scanning electron microscopes.

References

[1] Bohn CD, Muller CR, Cleeton JP, Hayhurst AN, Davidson JF, Scott SA, Dennis JS. Production of Very Pure Hydrogen with Simultaneous Capture of Carbon Dioxide using the Redox Reactions of Iron Oxides in Packed Beds. Ind Eng Chem Res 2008;47:7623-30.
[2] Imtiaz Q, Yuzbasi NS, Abdala PM, Kierzkowska AM, van Beek W, Broda M, Muller CR. Development of $MgAl_2O_4$-stabilized, Cu-doped, Fe_2O_3-based oxygen carriers for thermochemical water-splitting. J Mater Chem A 2016;4:113-23.
[3] Kierzkowska AM, Bohn CD, Scott SA, Cleeton JP, Dennis JS, Muller CR. Development of Iron Oxide Carriers for Chemical Looping Combustion Using Sol-Gel. Ind Eng Chem Res 2010;49:5383-91.
[4] Bohn CD, Cleeton JP, Muller CR, Chuang SY, Scott SA, Dennis JS. Stabilizing Iron Oxide Used in Cycles of Reduction and Oxidation for Hydrogen Production. Energ Fuel 2010;24:4025-33.
[5] Liu W, Dennis JS, Scott SA. The Effect of Addition of ZrO_2 to Fe_2O_3 for Hydrogen Production by Chemical Looping. Ind Eng Chem Res 2012;51:16597-609.
[6] Thursfield A, Murugan A, Franca R, Metcalfe IS. Chemical looping and oxygen permeable ceramic membranes for hydrogen production-a review. Energ Environ Sci 2012;5:7421-59.
[7] Yüzbasi NS, Kierzkowska AM, Imtiaz Q, Abdala PM, Kurlov A, Rupp JLM, Müller CR. ZrO_2-Supported Fe_2O_3 for Chemical-Looping-Based Hydrogen Production: Effect of pH on Its Structure and Performance As Probed by X-ray Absorption Spectroscopy and Electrical Conductivity Measurements. The Journal of Physical Chemistry C 2016;120:18977-85.
[8] Galinsky NL, Shafiefarhood A, Chen Y, Neal L, Li F. Effect of support on redox stability of iron oxide for chemical looping conversion of methane. Applied Catalysis B: Environmental 2015;164:371-9.
[9] Kidambi PR, Cleeton JP, Scott SA, Dennis JS, Bohn CD. Interaction of iron oxide with alumina in a composite oxygen carrier during the production of hydrogen by chemical looping. Energ Fuel 2011;26:603-17.
[10] Ishida M, Takeshita K, Suzuki K, Ohba T. Application of Fe_2O_3-Al_2O_3 composite particles as solid looping material of the chemical-loop combustor. Energ Fuel 2005;19:2514-8.
[11] Mattisson T, Johansson M, Lyngfelt A. Multicycle reduction and oxidation of different types of iron oxide particles application to chemical-looping combustion. Energ Fuel 2004;18:628-37.

[12] Wright JDSommerdijk NA, *Sol-gel materials: chemistry and applications*. Vol. 4. 2000: CRC press.
[13] Li F, Kim HR, Sridhar D, Wang F, Zeng L, Chen J, Fan L-S. Syngas chemical looping gasification process: oxygen carrier particle selection and performance. Energ Fuel 2009;23:4182-9.
[14] Barrett EP, Joyner LG, Halenda PP. The Determination of Pore Volume and Area Distributions in Porous Substances .1. Computations from Nitrogen Isotherms. J Am Chem Soc 1951;73:373-80.
[15] Brunauer S, Emmett PH, Teller E. Adsorption of gases in multimolecular layers. J Am Chem Soc 1938;60:309-19.